



HAL
open science

Simulation of atmospheric CO₂ over Europe and western Siberia using the regional scale model REMO

Anne Chevillard, Ute Karstens, Philippe Ciais, Sébastien Lafont, Martin Heimann

► **To cite this version:**

Anne Chevillard, Ute Karstens, Philippe Ciais, Sébastien Lafont, Martin Heimann. Simulation of atmospheric CO₂ over Europe and western Siberia using the regional scale model REMO. *Tellus B - Chemical and Physical Meteorology*, 2002, 54 (5), pp.872-894. 10.1034/j.1600-0889.2002.01340.x . hal-02923935

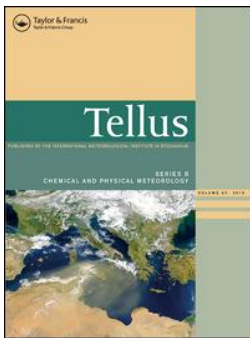
HAL Id: hal-02923935

<https://hal.science/hal-02923935>

Submitted on 29 Oct 2020

HAL is a multi-disciplinary open access archive for the deposit and dissemination of scientific research documents, whether they are published or not. The documents may come from teaching and research institutions in France or abroad, or from public or private research centers.

L'archive ouverte pluridisciplinaire **HAL**, est destinée au dépôt et à la diffusion de documents scientifiques de niveau recherche, publiés ou non, émanant des établissements d'enseignement et de recherche français ou étrangers, des laboratoires publics ou privés.



Simulation of atmospheric CO₂ over Europe and western Siberia using the regional scale model REMO

Anne Chevillard, Ute Karstens, Philippe Ciais, Sébastien Lafont & Martin Heimann

To cite this article: Anne Chevillard, Ute Karstens, Philippe Ciais, Sébastien Lafont & Martin Heimann (2002) Simulation of atmospheric CO₂ over Europe and western Siberia using the regional scale model REMO, *Tellus B: Chemical and Physical Meteorology*, 54:5, 872-894, DOI: [10.3402/tellusb.v54i5.16737](https://doi.org/10.3402/tellusb.v54i5.16737)

To link to this article: <https://doi.org/10.3402/tellusb.v54i5.16737>



© 2002 The Author(s). Published by Taylor & Francis.



Published online: 15 Dec 2016.



Submit your article to this journal [↗](#)



Article views: 52



View related articles [↗](#)



Citing articles: 11 View citing articles [↗](#)

Simulation of atmospheric CO₂ over Europe and western Siberia using the regional scale model REMO

By ANNE CHEVILLARD^{1*}, UTE KARSTENS², PHILIPPE CIAIS¹, SÉBASTIEN LAFONT³ and MARTIN HEIMANN², ¹*Laboratoire des Sciences du Climat et de l'Environnement, UMR CEA-CNRS 1572, F-91198 Gif-sur-Yvette, France;* ²*Max-Planck-Institut für Biogeochemie, D-07701 Jena, Germany;* ³*CESBIO, UMR CNRS-CNES-UPS, 18 av. E. Belin, Toulouse, France*

(Manuscript received 9 July 2001; in final form 13 June 2002)

ABSTRACT

The spatial distribution and the temporal variability of atmospheric CO₂ over Europe and western Siberia are investigated using the regional atmospheric model, REMO. The model, of typical horizontal resolution 50 km, is part of a nested modelling framework that has been established as a concerted action during the EUROSIBERIAN CARBONFLUX project. In REMO, the transport of CO₂ is simulated together with climate variables, which offers the possibility of calculating at each time step the land atmosphere CO₂ fluxes as driven by the modelled meteorology. The uptake of CO₂ by photosynthesis is calculated using a light use efficiency formulation, where the absorbed photosynthetically active solar radiation is inferred from satellite measurements. The release of CO₂ from plant and soil respiration is driven by the simulated climate and assumed to be in equilibrium with photosynthesis over the course of one year. Fossil CO₂ emissions and air–sea fluxes within the model domain are prescribed, whereas the influence of sources outside the model domain is computed from a boundary condition CO₂ fields determined a global transport model. The modelling results are compared against pointwise eddy covariance fluxes, and against atmospheric CO₂ records. We show that a necessary condition to simulate realistically the variability of atmospheric CO₂ over continental Europe is to account for the diurnal cycle of biospheric exchange. Overall, for the study period of July 1998, REMO realistically simulates the short-term variability of fluxes and of atmospheric mixing ratios. However, the mean CO₂ gradients from western Europe to western Siberia are not correctly reproduced. This latter deficiency points out the key role of boundary conditions in a limited-area model, as well as the need for using more realistic geographic mean patterns of biospheric carbon fluxes.

1. Introduction

The spatial and temporal distribution and variability of CO₂ are still poorly known over large parts of the globe. In the framework of the EUROSIBERIAN CARBONFLUX project the possibilities of inferring regional carbon fluxes over Europe and western Siberia from a combination of CO₂ measurements and

modelling efforts on different scales are investigated. For a long-lived trace gas like CO₂ the spatial distribution and temporal variation depends on the patterns of sources and sinks as well as on local and large-scale transport. To describe adequately all processes involved, a hierarchy of models, from global down to local scales, would be necessary. In this study we focus on the intermediate scale, using a regional mesoscale model of limited area, which covers most of the Eurosiberian continent (36×10^6 km²). Our model has a horizontal resolution on the order of 20–60 km and can resolve the heterogeneity of the surface and the meteorological processes in much greater detail than most present-day coarser global models. In order to run the

*Corresponding author.
e-mail: anne.chevillard@irsn.fr

Present affiliation: Institut de Radioprotection et de Sûreté Nucléaire, DPRE/SERGD/LEIRPA, B.P. 17, F-92262 Fontenay-aux-Roses, France.

limited area model, the large-scale meteorology has to be specified at boundaries and initial conditions, here taken from weather forecast analyses. Boundary conditions for tracers must be specified, and we prescribe them from the output of the global coarse-grid TM3 model.

Atmospheric transport of tracers can either be performed “on-line” as part of the atmospheric model which calculates the meteorology, or “off-line” by reading meteorological fields from analyses and re-computing subgrid scale processes. While the latter approach is less time-consuming and therefore widely used on global (Heimann, 1995; Ciais et al., 1997) and regional scales (e.g. Engardt and Holmén, 1999; Kjellström et al., 2002), the “on-line” transport modelling offers the possibility to couple consistently atmospheric transport and meteorology-driven biospheric sources (e.g. Denning et al., 1996). This gives access to the temporal variability of the meteorological fields at the time-step level, and thus allows us to compute biospheric fluxes at a fine inner day resolution.

In this study, we use the on-line regional scale atmospheric model REMO to simulate the transport of CO₂ in Europe and western Siberia. The modelling framework is described in Fig. 1. The model (two versions) is briefly described in section 2. In section 3, the sources and sinks of CO₂ which are used in the simulations, as well as boundary and initial conditions, are described. Special attention is given to net ecosystem exchange flux (NEE), driven by the model meteorology and satellite observations. The simulated NEE is

compared with eddy covariance flux tower measurements. In section 4, the results of the simulations are discussed for July 1998, and a more detailed comparison with atmospheric measurements is given in section 5. We selected measurements at 13 atmospheric stations, two short towers of flux measurements and two aircraft intensive sets of vertical profiles.

2. Model description

The REgional Model REMO is based on the Europamodell (EM) of the German Weather Service (DWD) (Majewski, 1991). For almost 10 years the Europamodell has been the operational regional weather forecast model of DWD. REMO has the possibility of using either the physical parameterisation package of EM or the same physics as the global climate model ECHAM-4 (Roeckner et al., 1996). Some sensitivity studies in different climatic regions were presented in Jacob and Podzun (1997).

The version of REMO (version 4.3) used in this study includes the DWD physical parameterisation package. The model uses the hydrostatic approximation with 20 vertical levels in a hybrid coordinate system with six layers below 1500 m. The horizontal resolution is 0.5° in a rotated spherical coordinate system, with the equator almost in the centre of the computational domain. This results in a horizontal grid size of roughly 55 km × 55 km. In the present study the model domain encompasses Europe and western Siberia

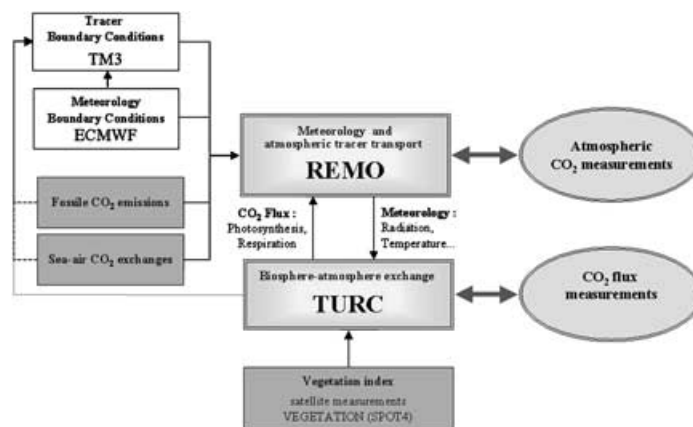


Fig. 1. Modelling framework to simulate biospheric fluxes and atmospheric CO₂ mixing ratios with the regional-scale model REMO. The modelled Net Ecosystem Exchange is compared with pointwise eddy covariance data, whereas the modelled CO₂ distribution is compared with atmospheric stations.

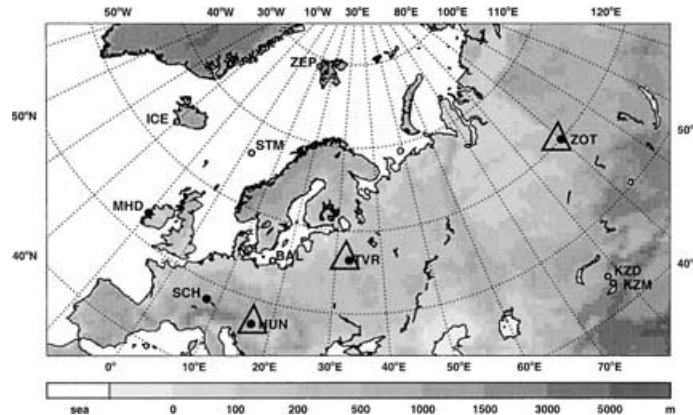


Fig. 2. The REMO model domain together with the sites used for the model-data comparison. Filled circles indicate continuous atmospheric CO₂ records, open circles flask sampling stations and triangles eddy covariance sites used in this study.

(Fig. 2) and covers an area of 36×10^6 km². Analyses of the European Centre for Medium-Range Weather Forecasts (ECMWF) are used as initial and boundary conditions for the meteorological part of the model. These boundary data are updated every 6 h.

The performance of REMO in simulating the atmospheric circulation on the regional scale has been investigated in several studies by comparing model results to different types of measurements. Most of the comparisons have been focused on water and energy budget components and related parameters (Karstens et al., 1996; Ahrens et al., 1998; Hollmann et al., 2000; Lindau, 2000; Hamelbeck et al., 2001; Jacob et al., 2001; Jürrens, 1999; Meijgaard et al., 2001; Rockel and Karstens, 2001; Zhang et al., 2001). The comparison studies all showed that REMO is capable of realistically simulating synoptic and subsynoptic features. They also give an impression of the uncertainties involved in atmospheric modelling and reveal specific differences between model results and observations, leading to further model development efforts. Because the meteorological part of REMO in the version used in this study is very close to the EM we can also rely on the continuous verification efforts of DWD (Schrodin, 1993–1999).

The model was extended to an on-line atmosphere-chemistry model by implementing modules for the transport of tracers and tropospheric chemical processes (Langmann, 2000). In REMO the tracer transport is represented by horizontal and vertical advection, vertical diffusion and convective transport. Advective transport is solved explicitly according to the algorithm of Smolarkiewicz (1983). Subgridscale

vertical turbulent fluxes are calculated following Louis (1979) in the surface layer and using a second order closure scheme (Mellor and Yamada, 1974) in the layers above. Vertical transport of tracers in convective clouds is parameterised in the same way as the transport of liquid water in the mass flux scheme by Tiedtke (1989). Tracer transport is calculated at every time step of the meteorology computation in the model.

In general, REMO can be operated in two different modes. In the “climate mode” (Jacob and Podzun, 1997) the model is initialised once and continuously forced at the lateral boundaries using either results obtained from a global climate model or analyses. In the “forecast mode” (Karstens et al., 1996), the results of consecutive short-range forecasts (30 hs) are used. REMO is started for each day at 00 UTC from weather forecast analyses and a 30-hour forecast is computed. To account for a spin-up time the first six hours of the forecast are neglected. This spin-up time has been shown to be sufficient for EM of DWD and is therefore assumed adequate also in the present study. By restarting the model every day from analyses, the model state is forced to stay close to the weather situation of these analyses. The tracer transport is calculated continuously like in the “climate mode”. This is done by simulating only the meteorology in the first 6 hours of each run and passing the tracer fields directly from the last time step of the previous 30-hour forecast.

In previous tracer transport studies (e.g. Langmann, 2000), which were focused on short episodes (several weeks), REMO was used in the forecast mode. However, the atmospheric transport of CO₂ should be studied on longer periods (several months to several years).

Table 1. Correlation coefficient between simulated and observed air temperature using two versions of REMO

	REMO forecast observations	REMO climate observations
SCH – 30 m	0.91	0.61
SCH – 130 m	0.93	0.63
TVR – forest	0.66	0.48
TVR – bog	0.81	0.56
ZOT – forest	0.84	0.44
ZOT – bog	0.77	0.47

We will therefore also investigate the performance of the model in the climate mode, which is computationally more efficient. In future scenario simulations, for instance to regionalise the impacts of climate change given by a global climate model output, the climate mode is more adapted.

Over the whole domain, the air temperature in July 1998 computed by the forecast mode is closer to the ECMWF analysis than the result of the climate mode. In the lowest level, the spatial average of the REMO minus ECMWF difference reaches 0.5 ± 2.3 °C in the climate mode, whereas it is only -0.05 ± 0.9 °C in the forecast mode. The comparison of the observed and simulated temperature time series at several stations shows a better correlation for the forecast mode (Table 1). The correlation coefficient between model and observations for the forecast mode is between 0.66 and 0.93, whereas it is only between 0.44 and 0.63 for the climate mode.

In the following analysis of CO₂, we will therefore present mainly the results of the forecast mode. In the comparison with measurements, we will, however, also include the result of the climate mode (as well as the global model TM3), in order to quantify the effect of different atmospheric transport and meteorology on the CO₂ mixing ratio. The differences between both modes are also discussed in section 4.4.

3. Model set-up for the fluxes and transport of CO₂

In order to analyse the effects of distinct sources that influence the CO₂ distribution, we transported separately the different components (biospheric, oceanic and anthropogenic) produced by sources inside the REMO domain and by external sources, which pene-

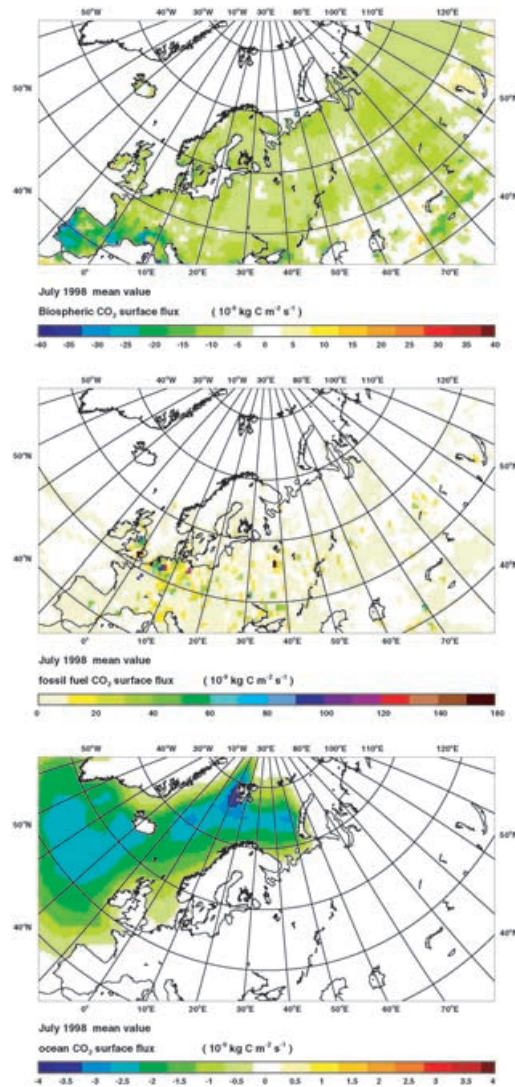


Fig. 3. Monthly fluxes in July 1998: net ecosystem exchange (NEE, upper panel), fossil fuel emissions (middle panel) and net sea-air fluxes (lower panel). Units are 10^{-9} kgC m⁻² s⁻¹.

trate into the domain through the lateral boundaries, as summarised in Fig. 1. Figure 3 shows the July 1998 monthly means of the biospheric, oceanic and fossil fluxes. The monthly mean biospheric flux in the REMO domain is estimated from the TURC model to be a net sink of -0.35 GtC in July 1998. The net uptake of CO₂ by the ocean within the model area is -0.05 GtC, and the total fossil emission is 0.17 GtC.

3.1. Vegetation–atmosphere exchanges (NEE)

The vegetation–atmosphere exchange of CO₂ is described by the TURC model, Terrestrial Uptake and Release of Carbon (Lafont et al., 2002; Ruimy et al., 1996). The TURC model estimates carbon uptake (photosynthesis) and release by vegetation and soil (respiration) from meteorological variables and satellite observations. Plant photosynthesis, or Gross Primary Production (GPP), is set to be in balance with the sum of plant respiration for growth and maintenance, and soil heterotrophic respiration over one year. The net biospheric flux (NEE), positive when CO₂ is released into the atmosphere, is the sum of all respiration terms minus photosynthesis. Photosynthesis depends on (1) *Rad*, incident solar global radiation, (2) *c*, the estimated fraction of *Rad* to be photosynthetically active, i.e. PAR (*c* = 45.6%), (3) *f*, the absorption coefficient of the canopy, a linear function of the NDVI (Normalised Difference Vegetation Index) computed from satellite observations of VEGETATION, a SPOT4 spaceborne instrument, (4) *ε*, the photosynthetic efficiency, ratio of canopy photosynthesis to the absorbed radiation and (5) *g*, a “freezing factor” that divides by two the GPP when daily average air temperature is lower than −2 °C during more than three consecutive days (Lafont et al., 2002).

$$GPP = A \times Rad \quad (1)$$

where $A = g \times \varepsilon \times f \times c$ is a daily coefficient. Autotrophic respiration is separated into growth (*RAg*) and maintenance fluxes (*RAm*). *RAm* depends linearly on the ambient air temperature [eq. (2)]:

$$RAm = A' \times T_{air} + B' \quad (2)$$

where *A'* and *B'* are daily functions of plant biomass. If daily GPP is larger than daily *RAm*, the remaining assimilates are used by plants for growth respiration [eq. (3)]. The coefficient *D* (=0.28 g g^{−1}) corresponds to the amount of glucose used to produce 1 g of dry matter (see Ruimy et al. (1996) for more details):

$$RAg = D \times (GPP - RAm)_{daily\ mean}. \quad (3)$$

The heterotrophic respiration (*RH*) is related to the deviation of the soil temperature (*T_{soil}*) from the reference temperature of 0 °C (*T₀*), according to a *Q₁₀* exponential relationship (*Q₁₀* = 2). The coefficient *V₀* in eq. (4) permits to decrease *RH* in wet soils and it is adjusted to equilibrate the net biospheric flux on an annual basis, which nevertheless restricts our analysis to seasonal or shorter time scales:

$$RH = V_0 \times Q_{10}^{\left(\frac{T_{soil}-T_0}{10}\right)}. \quad (4)$$

In this study we use two methods to obtain hourly fluxes from the daily estimations of TURC. In REMO climate mode, daily *A*, *A'*, *B'*, *V₀* and *RAg* are provided by Lafont et al. (2002). One preliminary run of REMO, without tracer transport, is performed to drive TURC with the meteorological data necessary for the determination of *V₀* and *RAg*. The fluxes are then determined simultaneously with atmospheric CO₂ transport in REMO, according to eqs. (1)–(4), using REMO meteorological fields at each time step (5 min). In REMO forecast mode, the diurnal variations of *GPP*, *RAm* and *RH* are parameterised according to the eqs. (1), (2) and (4). As this mode is strongly constrained by the ECMWF fields, daily mean biospheric CO₂ fluxes are determined using information from ECMWF analyses. The same procedure is also used in the global TM3 simulation that provides CO₂ boundary conditions to REMO (see section 3.2).

3.1.1. Sensitivity of NEE to the photosynthetic efficiency. We tested two sets of *ε* within the TURC model. The first set is from the original version of TURC by Ruimy et al. (1996), who used a uniform value of the *ε* parameter (0.020 mol CO₂ per mol PAR). The second set is from Lafont et al. (2002), who suggest, based on a compilation of recently published eddy flux tower measurements, that the original *ε* value is overestimated in bogs and boreal forests. The simulated NEE at Zotino (Central Siberia) is most affected by the lower *ε* values recommended by Lafont et al., in contrast with the two other sites. Using lower *ε* values greatly improved the TURC simulation there in July 1998, resulting in an important diminution (70%) of the daily NEE amplitude, whereas the monthly mean CO₂ sink is only reduced by 8%. At Fyodorovskoye (European Russia), both the monthly biospheric sink and the daily NEE peak-to-peak amplitude are reduced by 30%. At Hegyhátsál (Hungary), the monthly sink is doubled and the daily NEE amplitude stays constant. One can therefore anticipate that the atmospheric CO₂ concentration is sensitive to decreasing the value of the *ε* factor between Ruimy et al. (1996) and Lafont et al. (2002). On a monthly basis, the simulated average CO₂ mixing ratio decreases at the lowest level (6 ppmv smaller at Zotino and about 1 ppmv at the two other sites), whereas it increases at 500 m above the ground. This is mainly due to the “rectification” coupling between daily variations of biospheric fluxes and daily variations of the vertical mixing. In the

following, we only discuss results obtained with the ε values of Lafont et al. (2002).

3.1.2. Comparison with NEE measured by eddy covariance. We checked the TURC fluxes driven by REMO forecast mode against eddy covariance measurements of NEE (Net Ecosystem Exchange) at three specific locations (See Appendix A1). The forecast mode is here preferred because it is closer to the observed meteorology on a day-to-day basis. Two eddy covariance systems were installed over forest and bog vegetation at Fyodorovskoye and Zotino as part of the EUROSIBERIAN CARBONFLUX project (Fig. 2). In addition, we used NEE data over a cropland/woodland mosaic at Hegyhátsál in Hungary because a precise atmospheric CO₂ concentration record is also available at that site on top of a tall tower. Figure 4 compares the simulated NEE with eddy-flux

measurements. The simulated NEE represent a composite average over the REMO grid cell which contains a flux tower site. However, some large differences exist in NEE between two towers within the same grid cell, located over different vegetation types, due to subgrid heterogeneity. For instance, at Fyodorovskoye over a southern taiga area, the correlation between the measured NEE over a 150-yr-old spruce stand and over a bog distant from few kilometres is of 0.66 only. At Zotino, the correlation between NEE of a 220-yr-old pine forest stand and a bog nearby is of 0.69. Comparison between TURC driven by REMO and the eddy covariance NEE is therefore qualitative, but it can nevertheless provide a coarse check of the realism of the simulated fluxes, which is a prerequisite to obtain realistic atmospheric CO₂ fields. In Figure 4 we observe a large difference in the daily peak-to-peak amplitude of

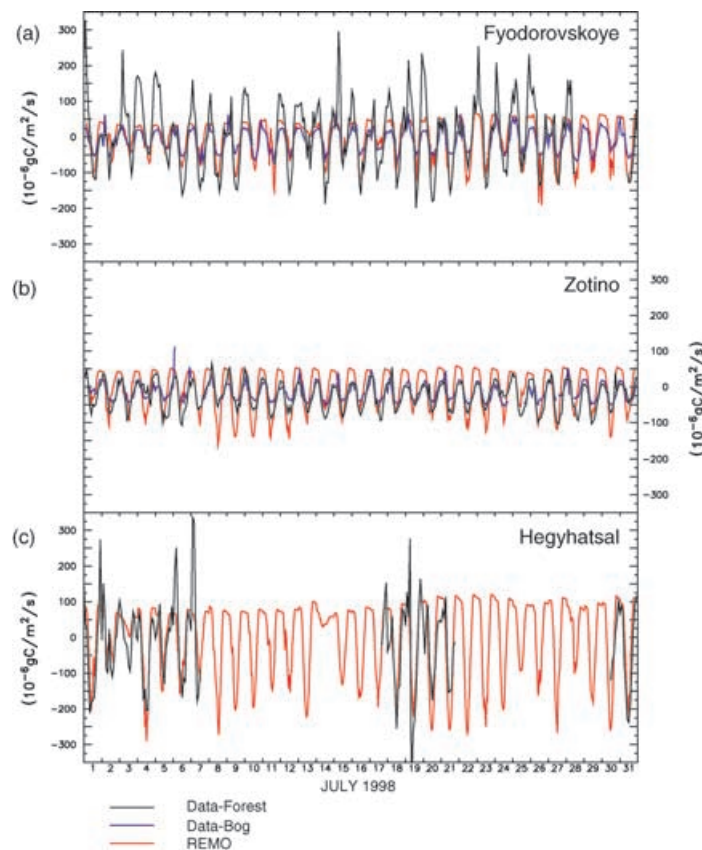


Fig. 4. Modelled (red) and observed (black) NEE along an East to West transect at Zotino (220-yr-old pine forest and nearby bog in central Siberia), Fyodorovskoye (150-yr-old spruce forest and nearby bog in European Russia) and Hegyhátsál (cropland and woodland mosaic in western Hungary).

Table 2. Monthly mean peak-to-peak amplitude of NEE (10^{-6} gC m $^{-2}$ s $^{-1}$)^a

NEE	REMO forecast	REMO climate	Observations
HUN	272.0 ± 89.7 (0.61)	280.4 ± 93.7 (0.60)	566.1 ± 303.6
TVR	145.1 ± 48.0 (0.71)	175.8 ± 61.5 (0.66)	359.1 ± 84.8
Forest			135.3 ± 55.5
Bog	(0.70)	(0.64)	
ZOT	150.1 ± 32.0 (0.76)	138.6 ± 33.6 (0.74)	130.8 ± 37.7
Forest			101.4 ± 43.7
Bog	(0.68)	(0.66)	

^aThe correlation coefficient between model and observations is indicated in parenthesis.

the measured NEE between the three sites, with higher amplitude in Hegyhátsál (566×10^{-6} gC m $^{-2}$ s $^{-1}$) and lower ones at Zotino (131×10^{-6} gC m $^{-2}$ s $^{-1}$ in forest and 101×10^{-6} gC m $^{-2}$ s $^{-1}$ in bog). The TURC model driven by REMO reproduces the variability of NEE on the East to West transect between Siberia, European Russia and Central Europe (Table 2). At Zotino, the modelled fluxes are of the same order of magnitude than the measured ones at the *Pinus sylvestris* site (correlation of 0.76 in Table 2). At Fyodorovskoye, the daytime simulated uptake matches reasonably well the spruce forest observations (correlation of 0.71 in Table 2), but the night-time simulated respiratory flux is lower than observed, and more comparable with measurements over the nearby bog. The measured respiration at the spruce site in Fyodorovskoye presents some nights (e.g. 19–20 and 23–28 July 1998) very large values as compared to the bog and to other days in forest (all flux data were corrected from storage terms using measured CO $_2$ profiles within the canopy). The REMO model is not able to reproduce such “events” (they do not occur at the Zotino forest site). At Hegyhátsál, similarly, very large night-time respirations occasionally observed are not reproduced in TURC (correlation of 0.61 in Table 2), but the maximum daytime carbon uptake is well simulated by the model.

3.2. Ocean–atmosphere fluxes and fossil fuel emissions

The sea-to-air flux of CO $_2$ is described according to Takahashi et al. (1999), who assembled and interpolated measurements of the sea minus air difference in CO $_2$ partial pressure (pCO $_2$) and estimated

monthly mean net fluxes using a wind speed dependent gas exchange coefficient (Wanninkhof, 1992). Regions of maximum CO $_2$ uptake by the ocean in July 1998 are located south of Spitzbergen and over the North Eastern Atlantic Ocean between Ireland and Southern Greenland (Fig. 3).

As fossil CO $_2$ emissions, we used the Emission Database for Global Atmospheric Research (EDGAR V2.0) of Olivier et al. (1996), which consists of global $1^\circ \times 1^\circ$ maps of emissions from industry, heating, transportation and cement manufacturing. For this database national CO $_2$ emissions are estimated using statistics on energy consumption (from IEA) and industrial production (from the United Nations) together with CO $_2$ -specific emission factors. The emissions are distributed within each country according to point-source and area-source information in combination with population density maps. Great Britain and Central Europe are the regions with highest emissions (Fig. 3). Only very few fossil sources are mapped north of 60° N, and there are almost no fossil sources in Northern Siberia. The EDGAR fossil CO $_2$ emission map corresponds to the year 1990. Changes in geographic emission patterns between 1990 and 1998 with a decrease in Eastern Europe and Russia have been reported (Marland et al., 2000) see Trends Online <http://cdiac.esd.ornl.gov/trends/trends.htm>. Emissions were stable between 1990 and 1998 over western Europe, but they decreased by 20% in Russia and Eastern Europe. No seasonal nor diurnal pattern is attributed to fossil CO $_2$ emissions, which are prescribed to the lowest model layer, assuming the maximum height at which industrial emissions are released to be 70 m.

3.3. Initial and boundary conditions

For a long-lived trace gas like CO $_2$, not only do local influences have to be accounted for in a regional simulation but also the role of sources and sinks outside the model domain is crucial. Therefore global CO $_2$ mixing ratio fields are needed as initialisation and at the lateral boundaries during the model run. The importance of boundary conditions in REMO simulations was already shown for a short-lifetime gas, radon-222 (Chevallard et al., 2002) and for ozone (Langmann and Bauer, 2001). In the present study, initial and boundary conditions are provided by the global transport model TM3 (Heimann, 1995). The TM3 model has a horizontal resolution of $4^\circ \times 5^\circ$ along with 19 vertical layers, and provides concentrations fields at 3-hr

intervals. To ensure consistency when nesting REMO into TM3, the CO₂ concentration is generated globally in TM3 with ECMWF transport fields that are identical to those used in REMO forcing. Similarly, the same set of CO₂ surface fluxes are used in REMO and TM3. In TM3, the diurnal cycle of NEE is constructed from TURC in the same way as described for REMO forecast, except that meteorological information from ECMWF analyses are used. The TM3 model does not provide an absolute concentration of CO₂. To compare model results to observations, we added an “offset” value, constant in time and space. This value (355 ppmv) has been determined such that the modelled CO₂ concentration is closest to the observations at 3000 m at Fyodorovskoye and Zotino during July 1998.

4. Results

We discuss here the patterns of the atmospheric CO₂ simulated by REMO in forecast mode. For each CO₂ component (fossil, biospheric and oceanic), we firstly present the mean horizontal distribution over Europe and Western Siberia, secondly the temporal variability, and thirdly we discuss the specific influence of the boundary conditions. The last point is focused on the comparison between REMO climate and REMO forecast simulations.

4.1. Modelled CO₂ spatial distribution

The REMO monthly averaged CO₂ for July 1998 is presented in Fig. 5 for each component within the Atmospheric Boundary Layer (ABL). The 300 m level roughly represents the average height of the ABL. The CO₂ distribution in this layer is not only dominated by the strong influence of the fluxes but also reflects the contribution of local and large-scale horizontal transport. It is immediately seen in Fig. 5b that the “classic” image of a north–south concentration gradient in latitude inferred from marine boundary layer measurements (Conway et al., 1994) leaves place to a more complex picture where east–west gradients between oceans and land are dominant. It is possible to evaluate separately the particular influence of each source to the overall CO₂ concentration. Over central Europe, higher CO₂ values are mainly caused locally by fossil fuel emissions (Figs. 5b and f). In Siberia, lower CO₂ values reflect on the other hand the vegetation sink (Figs. 5b and d). Over the continents, the overall

reduction of monthly CO₂ in the ABL (Fig. 5b) due to uptake by photosynthesis exceeds in the monthly mean the increase due to respiratory release. The biospheric sink reduces CO₂ in the boundary layer by approximately 2 ppmv in Central and Western Europe, and by 5 ppmv in Western Siberia as compared to the value over the ocean. We attribute this West to East negative gradient in biospheric CO₂ within the ABL mainly to the increasing exposure of air to uptake by plants under the dominant westerly circulation. Note that “exposure” only occurs during daytime when the 300 m level is directly connected to the surface fluxes by vigorous mixing in the ABL. Interestingly, the simulated negative east minus west gradient at 300 m (Fig. 5d) is of opposite sign than the east minus west difference in NEE (Fig. 3), which shows less uptake in the east than the west.

In the western corner of the model domain (Fig. 5b), one can also detect the influence of uptake by vegetation over North America, which is advected across the North Atlantic towards Europe. This illustrates the importance of atmospheric transport acting on sources from outside the model area (Chevallard et al., 2002). The influence of the North Atlantic ocean sink on the CO₂ concentration at 300 m over the continents is smaller than the one of the vegetation sink, but it is not negligible. Ocean uptake alone causes a reduction of CO₂ concentration over north-western Europe and Scandinavia of –0.5 ppmv as compared to the interior of Siberia.

At 30 m, the influence of the biospheric CO₂ component results in average concentrations higher than just above (Figs. 4c and d). This effect results from the covariance between NEE and vertical mixing in the atmospheric boundary layer: at night, respired CO₂ accumulates in the shallow nocturnal boundary layer, whereas, during the day, the signal of photosynthetic uptake is diluted over a deeper, often convective, air column (Denning et al., 1996). In contrast, a source with no diurnal variation, such as fossil fuel combustion or air sea exchange results in a contribution of the same sign on the CO₂ distribution at every altitude: positive for the fossil emissions (Figs. 5e and f) and negative for the ocean uptake (Figs. 5g and h).

4.2. Modelled CO₂ temporal variability

Figure 6 illustrates the temporal variability of CO₂ in REMO, at three sites (Fig. 2): Schauinsland in western Europe, Fyodorovskoye in western Russia and Zotino in central Siberia. In the ABL, both at 30 and

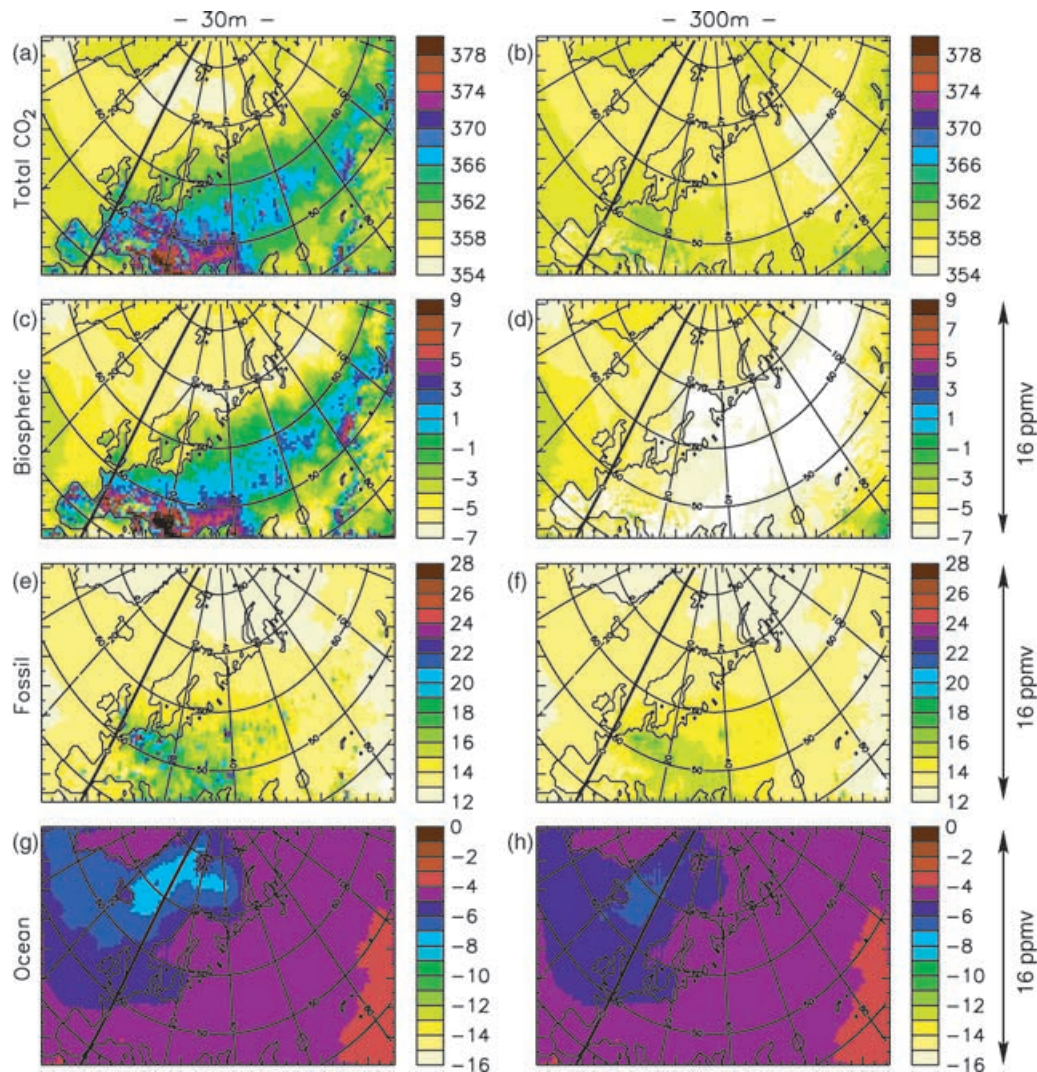


Fig. 5. Monthly means simulated CO₂ mixing ratio (in ppmv) in July 1998 in the boundary layer at 30 m and 300 m above ground, the first two model vertical layers in REMO. (a) Total CO₂ defined as the sum of fossil, biotic and ocean contributions of sources within the domain and of boundary conditions to which an arbitrary offset value of 355 ppmv is added. (b) Biospheric CO₂ resulting from photosynthesis uptake and plant and soil respiration, including its boundary conditions. (c) Fossil CO₂. (d) Ocean CO₂.

300 m, the CO₂ temporal variability is clearly driven by the terrestrial biosphere, and it is associated with a very strong diurnal cycle. In summer, the mean diurnal change in the biospheric CO₂ component is induced by the covariance between NEE and vertical mixing in the atmospheric boundary layer (see above). At 300 m, the daily amplitude of the biospheric CO₂ component is much smaller than at 30 m and its phase is slightly

shifted, approximately by 2 h. Near the surface, the maximum of CO₂ is observed in the early morning (at 5:00 AM) at Fyodorovskoye and Zotino. Generally, maximum release by respiration occurs about 2 h before the corresponding signal in CO₂ concentration. The change in ABL depth occurs before the variations of the biospheric fluxes. In the lowermost free troposphere, on the other hand, the variability in

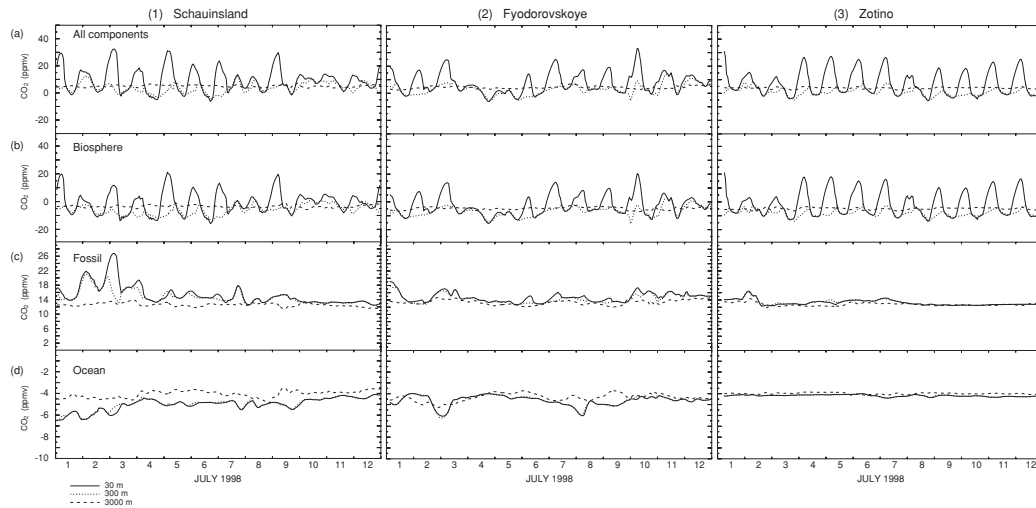


Fig. 6. Modelled and observed CO₂ time series at Schauinsland (southern Germany), Fyodorovskoye (European Russia) and Zotino (central Siberia) during July 1998. (a) Total CO₂, (b) biospheric, (c) oceanic, (d) fossil components are shown separately at 30 m (solid line), 300 m (dotted line) and 3000 m (dashed line).

CO₂ concentration (Fig. 6) is much smaller than in the boundary layer, but is still dominantly influenced by the biospheric component.

The diurnal variability caused by the fossil CO₂ component, albeit lower than the one due to biospheric CO₂, is yet stronger at stations which are close to fossil fuel sources: Schauinsland and Fyodorovskoye (Fig. 6). Because in our simulation the fossil emissions are prescribed constant in time, the diurnal variation in the fossil CO₂ component reflect only temporal changes in the transport. Note that, in order to produce a nocturnal increase in the fossil CO₂ component at a given station, one needs fossil emissions in the vicinity of that station in the REMO model. In the “pristine” air of Siberia at Zotino, even though vertical transport varies between day and night, there is no daily cycle in fossil CO₂ (Fig. 6c).

The diurnal variability of the ocean sink component gets strongly dampened over the interior of continents. At Schauinsland, in western Germany, there is no discernible diurnal variation of that component, whereas at Mace Head (not shown), the peak-to-peak amplitude of the ocean induced diurnal variation in CO₂ is of 1 ppmv, a small signal as compared to the diurnal effect of the biosphere at this marine station.

It is also interesting to analyse the modelled variations in the daily cycle of atmospheric CO₂ from one day to the next. At Zotino for instance, during July 1998, the REMO model produces a fairly regular di-

urnal cycle with an amplitude of 20–25 ppmv near the surface and of 4–7 ppmv at 300 m. The Zotino area is under the influence of stationary high-pressure systems most of the time. In high-pressure regions the ABL usually shows a very well defined structure with a turbulent mixed layer during the day and a shallow stable nocturnal boundary layer with a residual layer aloft containing former mixed layer air (Stull, 1988). Only on some occasions (e.g. July 8) do passing low-pressure systems cause a reduction of the diurnal amplitude of biospheric CO₂ due to stronger and higher reaching turbulent mixing, especially during the night. At Fyodorovskoye and Schauinsland, the diurnal cycle amplitude of the biospheric component is more irregular than at Zotino. Both stations are more frequently influenced by the alternance of passing frontal systems and periods of high pressure. A comparison of the simulated surface pressure with the observed pressure (not shown) shows that the model is reproducing this sequence with a correct timing. During periods of high pressure the daily amplitude of the biospheric CO₂ component is larger compared to Zotino, reaching up to 40 ppmv at Fyodorovskoye and 50 ppmv at Schauinsland. In these situations the local conditions and the vertical exchange are mainly determining the CO₂ distribution. During the passage of frontal systems, synoptic scale turbulence dominates the fluctuations of the CO₂ concentration. At 300 m, the diurnal variations are less regular than the ones closer to the

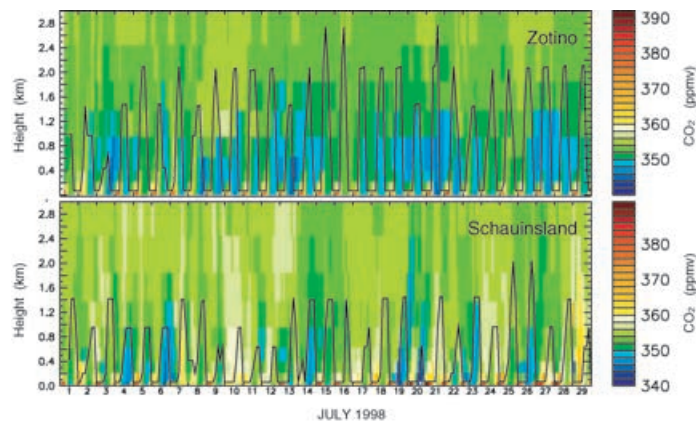


Fig. 7. Modelled time series of the vertical variability of CO₂ within the atmospheric boundary layer and the lower troposphere at Zotino and Schauinsland. The simulated boundary layer height is indicated by a black line. Note the nocturnal accumulation of respired CO₂ near the surface and the daytime dilution of plant uptake by convection.

surface. This indicates that the CO₂ concentration is, at this height, more strongly influenced by the large-scale synoptic transport.

Time series of the vertical CO₂ distribution in the lowest 3000 m of the troposphere are shown for Zotino and Schauinsland in Fig. 7, together with estimates of the ABL height. The correlation between the sign of biospheric fluxes and ABL turbulence results in a time-mean vertical CO₂ structure with: (1) a layer of comparatively low CO₂ concentrations in the planetary boundary layer due to photosynthesis and (2) higher values near the surface due to respiration. CO₂ depleted air is mixed up in the daytime ABL compared to CO₂ enriched air during stable conditions at night. Above the ABL the CO₂ distribution is mainly influenced by the large scale transport and much less variable. At Zotino, where high-pressure situations with a regular diurnal cycle of turbulence in the ABL are prevailing, the separation between CO₂ enriched air near the surface and CO₂ depleted air above is clearly visible (Figure 7). At Schauinsland, the stronger vertical exchange caused by the larger-scale turbulence connected to the passing low-pressure systems is reflected in the CO₂ concentration pattern.

4.3. Influence of boundary and initial conditions

The simulated CO₂ concentration in each grid cell results from the superposition of (1) CO₂ emitted from sources inside the model domain, (2) CO₂ transported across the lateral boundaries, and (3) CO₂ introduced at the initialisation. Initial and boundary concentra-

tions both represent the contribution of the global emissions in the TM3 simulation, after steady state has been approached (4 yr). Initial and boundary conditions for the simulation of CO₂ were transported in this study as three separate components. For instance, one can see, in Fig. 8, that the fossil fuel component almost entirely reflects the influence of emissions from outside the model domain and prior to the start of the simulation. Initial conditions clearly dominate the signal during the first 6 d and afterwards are gradually replaced by information from the boundaries conditions (Figs. 8a and b). Conversely, at stations closer to the boundaries the influence of initial conditions is of shorter duration, e.g. 3 d only at Mace Head.

On the other hand, the biospheric component at Zotino is largely influenced by internal sources. In the lowest level, the contribution of initial and boundary conditions is small (Fig. 8c). Above the ABL, the influence of internal sources decreases and initial and boundary conditions become more important, while the temporal variability is of similar amplitude in all components (Fig. 8d). In general, the average CO₂ above the ABL is determined by short-term initial and boundary conditions, whereas temporal variations are equally influenced by internal and external sources. Within the ABL, local sources have a dominant influence.

4.4. Comparison between REMO “forecast” and REMO “climate”

In this part, we study the difference between the two modes of REMO (climate and forecast) on the

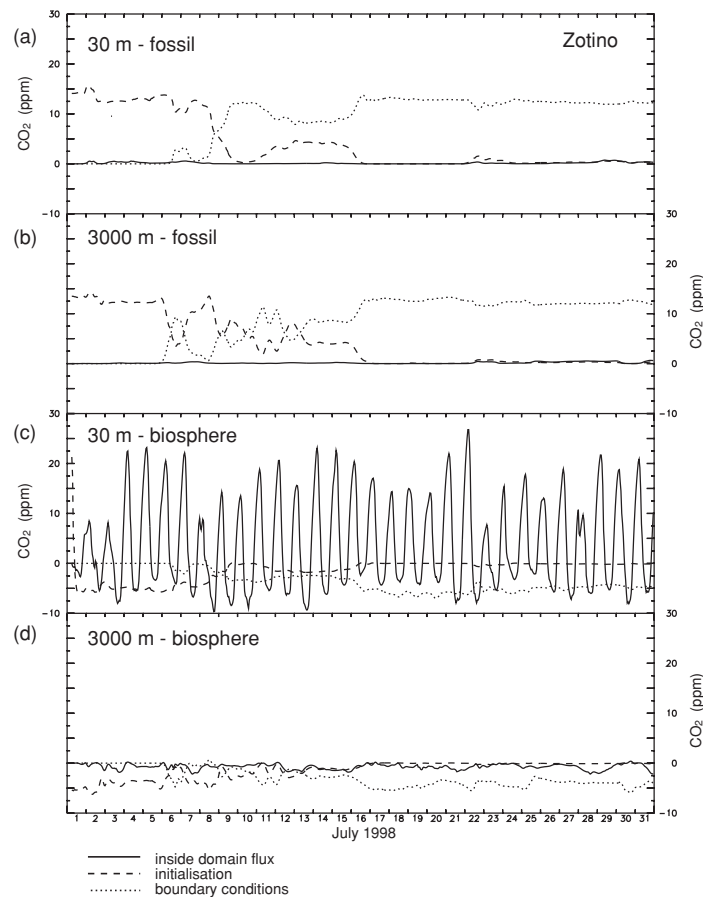


Fig. 8. Illustration of the role of initial and boundary conditions with respect to transport of sources within the domain at Zotino (central Siberia). (a) Fossil CO₂ time series at 30 m. (b) Fossil CO₂ time series at 3000 m. (c) Biospheric CO₂ at 30 m. (d) Biospheric CO₂ at 3000 m.

simulated CO₂ concentrations. The version of REMO run in climate mode is initialised on 1 March 1998 and computes its own climate, contrarily to REMO run in forecast mode which is readjusted everywhere each day to the ECMWF analysis. The climate and ancillary atmospheric tracer transport are consequently different between the two versions of the same model.

Overall, differences in monthly mean CO₂ concentration simulated by both model versions are large in the centre of the domain. Close to the lateral boundaries, the concentrations are very similar, consequences of (1) the same 6 hourly forcing by ECMWF fields and (2) the same 3 hourly prescribed CO₂ concentration fields from the global model TM3. On average over the whole domain, the CO₂ concentration

difference between climate and forecast modes is 1.0 ± 1.1 ppmv close to the surface and 0.6 ± 0.4 ppmv at 500 m above ground.

First, a comparison of monthly fossil and oceanic CO₂ components is performed (not shown), since those components have identical surface sources in both REMO modes. In the REMO-climate simulation, the oceanic CO₂ is spread out from the North Atlantic towards Scandinavia and northern Russia, in the lowest model layer, whereas it stays centred over the North Atlantic in the REMO forecast mode. This reflects a stronger westerly transport in REMO climate. Similarly, the fossil CO₂ component at 3000 m in REMO climate is more widespread towards the east (western Siberia), than in the REMO forecast run. At 300 m

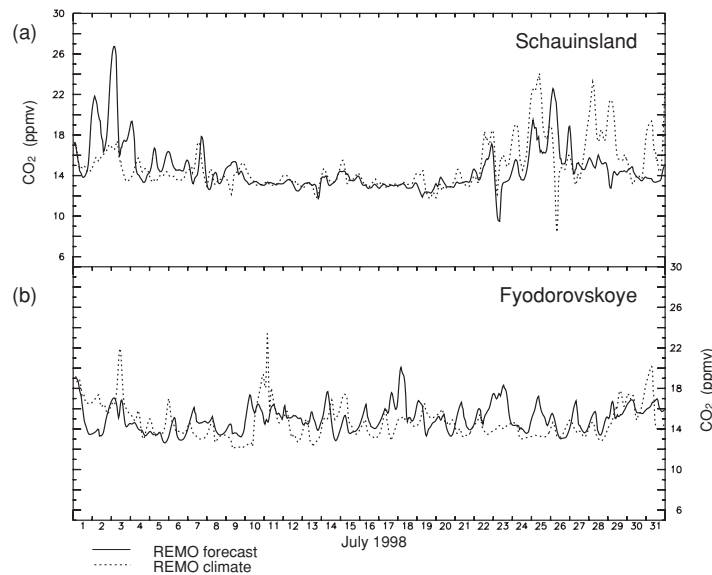


Fig. 9. Illustration of the differences between two versions “forecast” and “climate” of REMO. Time series of fossil CO₂ simulated by both versions of the model are given (a) at Schauinsland and (b) at Fyodorovskoye.

over Europe, where long range transport processes have a smaller influence on the fossil concentration than short range transport acting on nearby sources, both REMO climate and REMO forecast simulations give fairly similar results.

Figure 9 shows the time series of fossil CO₂ concentrations simulated by both versions of REMO at Schauinsland and Fyodorovskoye. At Schauinsland, a mountain station near an industrial emission area, fossil CO₂ transported by REMO forecast is very close to the one simulated in REMO climate over the period of 9–20 July 1998, whereas both model versions differ elsewhere. The period when both model versions agree corresponds to the passage of a frontal system with high winds, during which the influence of boundary conditions (similar in both model versions) is dominantly felt at Schauinsland. On the other hand, intervals when the model versions disagree correspond to the establishment of more local conditions. At Fyodorovskoye, that is located further away from industrialised emissions, the diurnal cycle of fossil CO₂ has a smaller amplitude than at Schauinsland in both versions of REMO (Fig. 9a). The variability of fossil CO₂ time series in the two versions is however very different, because far from the lateral boundaries, REMO in climate mode generates a distinct meteorology.

In the following comparison with measurements, results of REMO in the forecast mode are presented, since its simulated meteorology is closer to the observations. Lafont et al. (2002) showed in their study that the meteorological input fields used in TURC have a strong influence on the spatial and temporal patterns of the simulated NEE. Nevertheless, the comparison shows that, even in the climate mode, the model gives a realistic representation of the temporal and spatial characteristics of atmospheric processes (section 2) and tracer transport.

5. Comparison with atmospheric CO₂ measurements

5.1. Modelled and observed CO₂ variability at different stations

Time series of simulated CO₂ concentrations are compared with measurements (Fig. 10) during July 1998 at five different sites: Mace Head (coastal station), Schauinsland (mountain station), Hegyhátsál (tall tower) and Fyodorovskoye and Zotino (two short towers at each site with concentration records above forest and bog canopies). A caution flag should be raised regarding comparison between model

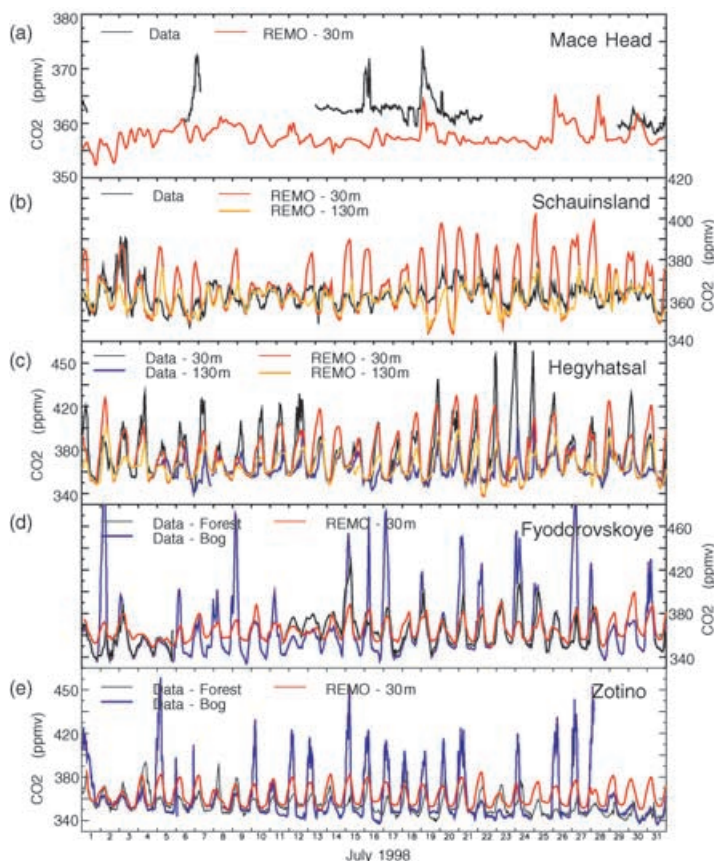


Fig. 10. Observed and simulated (red) atmospheric CO₂ mixing ratios from the North Atlantic Ocean to central Siberia at Mace Head, Schauinsland, Hegyhatsal, Fyodorovskoye and Zotino. At Fyodorovskoye and at Zotino, the observations are shown both over a bog at 8 m (blue) and forest canopy at 30 m (black) that are located within the same model grid cell. Red line, REMO simulation at 30 m above model ground; orange line, REMO at 130 m a.m.g.

observations at only a few stations: this approach is necessary but not sufficient for a comprehensive model verification. Besides, although stations are generally chosen to be representative of large regions, CO₂ may be influenced by local conditions, not accounted for in a model of average grid size of 55 km.

The observed CO₂ concentration at Mace Head exhibits a stable marine baseline over which are superimposed CO₂ peaks of 10 ppmv (6, 15 and 18 July). Those peaks lasting from a few hours up to a few days are related to sudden changes in the wind direction from well established west direction (ocean) to south or east (land) and to a decrease in wind speed. A rapid increase of the wind speed, associated with a return to westerly winds, brings back the CO₂ concentration

to the baseline value. The simulated standard deviation of CO₂ is about half the observed value (Table 3). Only the peak of 18 July is reproduced by REMO (Figure 10a), which explains the poor model data correlation in Table 4. 18 July is the longest and best defined synoptic “event” in July, for which the wind speed and direction changes are exactly reproduced by the model. The CO₂ emitted inside the REMO domain by the biospheric source is the only component that contributes to this peak. The amplitude of the peak is, however, underestimated (by 5 ppmv). On the other hand, two shorter duration peaks in 6 and 15 July are not represented in REMO because they correspond to very local conditions (wind speeds $<5 \text{ m s}^{-1}$) that are not resolved at the model’s resolution, a mismatch also

Table 3. Monthly means and standard deviation of CO₂ mixing ratio (ppmv)

Atmospheric CO ₂	REMO forecast	REMO climate	TM3	Observations
MHD	357.4 ± 1.5	360.7 ± 0.8	357.0 ± 1.6	362.4 ± 2.8
SCH–30 m	366.9 ± 11.1	366.9 ± 9.7	368.4 ± 12.1	362.3 ± 5.7
SCH–130 m	360.9 ± 5.3	362.4 ± 5.7	363.3 ± 4.5	
HUN–30 m	376.3 ± 20.1	377.2 ± 18.6	371.6 ± 5.9	372.5 ± 18.6
HUN–130 m	365.6 ± 11.0	367.9 ± 10.4	363.6 ± 5.4	361.8 ± 8.8
TVR–forest	364.4 ± 9.4	367.1 ± 9.1	367.2 ± 10.3	362.8 ± 15.5
ZOT–forest	362.8 ± 8.9	367.6 ± 9.0	361.9 ± 8.5	353.0 ± 8.9

Table 4. Monthly mean peak-to-peak amplitude of CO₂ mixing ratio (ppmv)^a

Atmospheric CO ₂	REMO forecast	REMO climate	TM3	Observations
MHD	3.2 ± 1.9 (0.35)	2.5 ± 1.5 (0.20)	2.2 ± 1.0 (0.09)	4.3 ± 3.4
SCH – 30 m	30.5 ± 10.5 (0.42)	26.3 ± 12.7 (0.38)	27.5 ± 17.4 (0.32)	12.6 ± 6.5
SCH – 130 m	13.8 ± 5.2 (0.30)	12.4 ± 6.1 (0.22)	11.5 ± 3.5 (0.25)	
HUN – 30 m	51.6 ± 17.6 (0.30)	46.3 ± 14.8 (0.50)	35.8 ± 19.4 (0.67)	52.8 ± 20.9
HUN – 130 m	27.7 ± 11.6 (0.51)	25.0 ± 11.7 (0.46)	13.0 ± 5.8 (0.41)	27.2 ± 10.4
TVR Forest Bog	24.2 ± 7.9 (0.73) (0.61)	25.1 ± 6.2 (0.62) (0.59)	23.6 ± 9.4 (0.74) (0.70)	39.5 ± 16.0 84.9 ± 40.1
ZOT Forest Bog	25.2 ± 4.6 (0.51) (0.64)	24.8 ± 6.4 (0.41) (0.55)	22.3 ± 8.2 (0.61) (0.77)	24.1 ± 10.2 59.2 ± 34.4

^aThe correlation coefficient between model and observations is indicated in parenthesis.

confirmed by ²²²Rn simulations in Chevillard et al. (2002). At Mace Head, the simulation of CO₂ depends much on the quality of the wind fields. For this study, we found that it is preferable to screen out local “events” (Biraud et al., 2002) from the observed record when trying to invert CO₂ fluxes using an atmospheric transport model.

At Schauinsland, the observed CO₂ diurnal cycle is small as compared to short towers just above the canopy. In the afternoon, the mountain station is in the well mixed ABL: photosynthesis exceeds respiration and the air is depleted in CO₂. During the night, formation of a shallow nocturnal boundary layer prevents the air enriched in CO₂ by respiration from reaching the mountain station. Therefore, biotic exchange controls the CO₂ daily cycle, but, when the station is influenced

by local conditions (e.g. 1–4 July), regional fossil CO₂ can also significantly contribute to it (Fig. 6c). The altitude of the station is 1205 m a.s.l., whereas the model ground is 700 m a.s.l. high, and one can therefore wonder what is the most adequate vertical location of the station in the model. Comparison between observed and modelled CO₂ suggests that the layer at 130 m above ground (830 m a.s.l.) would best match both the daily amplitude and monthly mean value of CO₂ (Table 3). Yet, the phase of the daily CO₂ oscillation is more realistic cycle at 30 m (Table 4), as is the simulated ²²²Rn amplitude (Chevillard et al., 2002). Differences between both model layers (up to 30 ppmv) occur only during the night (Fig. 10b), when respiration increases CO₂ near the ground. The afternoon CO₂ values at both 30 and 130 m are similar, due to

strong turbulence in the ABL. We thus recommend the use of only selected mid-afternoon data in REMO, because they can be more robustly reproduced by either of the first two model layers. Night-time accumulation effects at a mountain station are almost impossible to simulate realistically when the model resolution is smoother than the observed topography.

At the tall tower in Hegyhátsál, CO₂ is measured at respectively 10, 48, 82 and 115 m (Appendix). We compared REMO at 30 m (respectively at 130 m) with observations interpolated (respectively extrapolated) between the bracketing measurement heights assuming a logarithmic profile of CO₂. The data show a large diurnal oscillation with a higher night-time maximum by 25 ppmv at 30 m compared to 130 m, as implied by strong gradients of respired CO₂ near the ground under stable nocturnal conditions. Both levels, however, show similar CO₂ mixing ratios which differ by less than 1.2 ppmv during mid-afternoon when the ABL is well mixed. At 130 m, REMO reproduces well the observed variability (Table 3), and the phase and amplitude of the diurnal cycle (data not shown). At 30 m, the modelled phase signal is realistic, but the simulated nighttime maximum (at 06:00) is underestimated by 15 ppmv. Given the fact that the simulated nocturnal respiration is correctly matching the local eddy covariance data (Fig. 4), we can conclude that the night-time vertical mixing in REMO is too strong. Similar conclusions were independently obtained based on ²²²Rn in Chevillard et al. (2002). In summary, we found that the simulated daytime CO₂ on a tall tower can be robustly compared to observations at each height of the profile. In contrast, the simulated night-time CO₂ can only be safely compared with data if the tower reaches up high enough. This suggests that tall towers are much more valuable than short towers in providing systematic data for CO₂ sources and sink inferences in atmospheric transport models.

At Fyodorovskoye, CO₂ shows a large diurnal oscillation over the spruce forest canopy (40 ppmv). Note, however, that CO₂ is measured at this site to evaluate the night-time storage terms affecting NEE (Milyukova et al., 2002), and thereby it is not precisely calibrated against air standards as done at atmospheric stations. The accuracy of CO₂ measurements on top of flux towers at Fyodorovskoye and Zotino is estimated to be on the order of 10 ppmv (Milyukova et al., 2002). Nevertheless, such data are useful to compare with REMO for the phase and typical amplitude of the daily signal. The observed nocturnal CO₂ built-up over the bog is huge (ampli-

tude 85 ppmv), but the bog tower is too close to the ground (8 m) to allow proper comparison with REMO. This is confirmed by a higher correlation between modelled CO₂ and observed CO₂ at the forest tower (30 m) than at the bog tower (Table 4). Figure 10d shows that REMO underestimates the daily amplitude of CO₂ over the forest canopy (Table 3), which is not surprising because the amplitude of the modelled NEE is also underestimated. In fact, the spruce forest stand is a source to the atmosphere on a daily average even during July because of the site history (Milyukova et al., 2002), a feature that can not be captured within the simplified annually balanced TURC diagnostic model.

At Zotino, the daily oscillation of CO₂ above the pine forest canopy shows a lower peak-to-peak amplitude (24.1 ppmv) than at Fyodorovskoye. This reflects a smaller peak-to-peak amplitude of NEE (130.8 μgC m⁻² s⁻¹ against 360 μgC m⁻² s⁻¹ at Fyodorovskoye) as well as differences in vertical mixing between Central Siberia and European Russia. Inspection of the ratio between the amplitude of NEE and the amplitude of CO₂ above the canopy at both sites suggests that the nocturnal stability of the boundary layer is more pronounced (or more frequent) in central Siberia than in European Russia, where more frontal systems reach the site and break down the nocturnal stratification. As for Fyodorovskoye, we discarded comparison between REMO and the bog CO₂ measurements at 8 m above ground. Figure 10e shows that REMO correctly reproduces the amplitude of the daily cycle in CO₂ (Table 4), and even some of the synoptic variations, such as the persistent decrease in daytime CO₂ minima between 15 July and 20 July.

5.2. Modelled and observed CO₂ diurnal variability in vertical profiles

In order to investigate the performances of REMO in simulating the vertical variability of CO₂, the model results are compared with measured CO₂ vertical profiles. During the EUROSIBERIAN CARBONFLUX project, aircraft measurements of CO₂ concentration profiles were performed at Fyodorovskoye and Zotino in July 1998 three times a day during intensive campaigns (Ramonet et al., 2002; Lloyd et al., 2002; Styles et al., 2002). We use here continuous vertical CO₂ profiles sampled from 10 m up to 3000 m during several consecutive days in July 1998.

A comparison of REMO with vertical profiles is given in Fig. 11. The time-varying vertical structure of

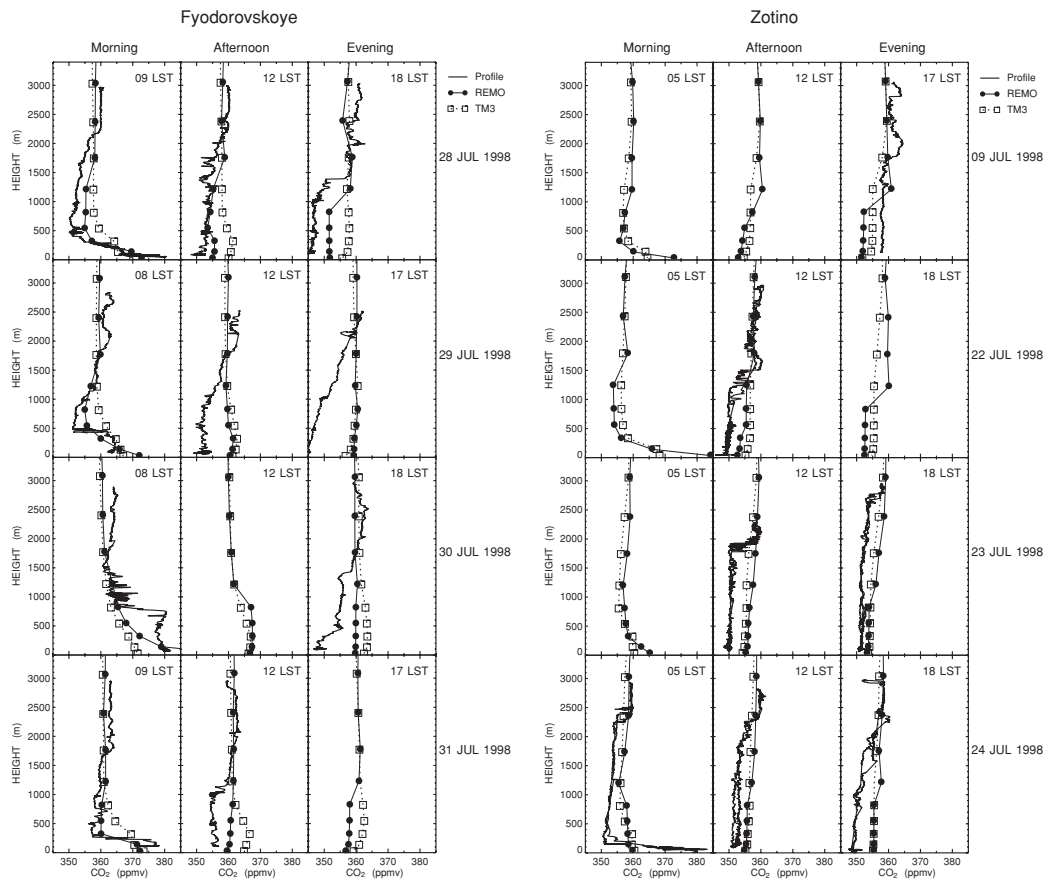


Fig. 11. Observed and modelled vertical profiles of CO₂ during an intensive period of observation in July 1998 where aircraft in-situ CO₂ vertical profiles were sampled in the morning, early afternoon and evening. Simulations by the fine resolution model REMO and by the coarse resolution model TM3 are represented. Left, Fyodorovskoye intensive campaign (28–31 July); right, Zotino intensive campaign (9–24 July).

simulated CO₂ at Zotino in July 1998 is also presented in Fig. 7. In Figure 11 the profiles are arranged in such a way that morning, early afternoon and evening flights at each site are grouped together. REMO has nine layers of increasing thickness between the surface and 3000 m.

For the two intensive aircraft campaigns, the measurements show similar variability with small CO₂ variations at 3000 m and large diurnal changes within the ABL. The CO₂ concentration in the upper part of the profiles (near 3000 m) that is representative for the free troposphere is used to determine a constant offset value. In general, the morning profiles show an accumulation of respired CO₂ near the surface below 500 m and a sharp decrease of the concentration above. At noon, the CO₂ profiles are much more uniform. In the

afternoon, the cumulated net uptake by the vegetation reduces the concentration, and daytime mixing transports the air depleted in CO₂ higher up. In the evening the CO₂ concentration in the lower part of the profiles is further reduced, and on some days CO₂ is increasing with height in the ABL when convection has stopped.

REMO is able to reproduce realistically the diurnal variation in the CO₂ vertical profiles (Fig. 11). In many cases, however, the reduction of CO₂ during the day is not strong enough compared to the measurements. Possible explanations could be that the net uptake of CO₂ by the vegetation is underestimated in the model (not so clear from Fig. 3) or that the vertical mixing in the model is too strong. We favour this latter hypothesis, since it can be seen that the sharp gradients across the top of the daytime

convective ABL cannot be reproduced in REMO. Additional inspection of the virtual potential temperature and humidity profiles with measurements shows that, during days when a clearly defined convective ABL develops in the model (e.g. 28 July in Fyodorovskoye and 9 July in Zotino), the CO₂ concentration within the ABL is strongly reduced by approximately 10 ppmv compared to the atmosphere above. One has to keep in mind that the aircraft profiles reflect in the lower part more local fluxes, whereas the model always represents an average for a 55 km × 55 km grid box. For a more reliable interpretation of the ability of REMO to simulate the vertical structure of the CO₂ concentration, more profiles under different conditions would be needed.

5.3. Modelled and observed monthly average CO₂ gradients among stations

We compare in Fig. 12 the simulated monthly averaged CO₂ mixing with observations. Some stations (Appendix and Fig. 2) are continuous sites, which of-

fer an accurate determination of the monthly mean CO₂ value within an instrumental error on the order of 0.1 ppmv (ZEP, SCH, HUN, MHD). We do not use here continuous records on short towers of eddy covariance measurements (TVR, ZOT), since those data are not calibrated, although they proved informative to study the variability (section 5.1). Other stations are discrete sampling sites, mainly from NOAA/CMDL, where flasks are collected approximately each week (ICE, STM, BAL, KZD, KZM). Monthly average CO₂ is computed in that case from a smoothed fit to the weekly flask data in the GLOBALVIEW-CO₂ (2001) data product. The error bar in Fig. 12 represents the standard deviation of individual flask data from the fit. Finally, we also have four aircraft sites (ORL, TVR, SYK, ZOT) where flasks are collected every 2–3 wk in the lower troposphere below 3000 m. We computed monthly average CO₂ values from aircraft data using the same procedure as for ground flask stations, except that the smoothed-fit curve was obtained using all flask samples between 2000 and 3000 m.

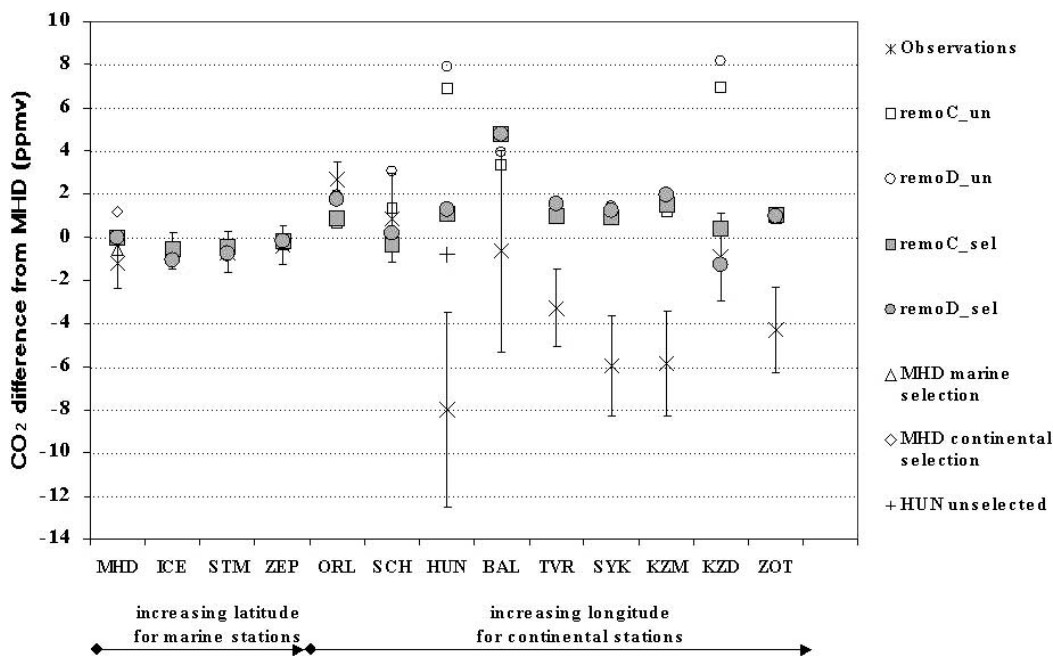


Fig. 12. Mean gradient of CO₂ between the North Atlantic ocean and Central Siberia. The first four marine stations are sorted as a function of increasing latitude. The nine remaining continental stations are sorted as a function of eastward increasing longitude. Comparison between observations (crosses with error bars) and REMO selected (respectively unselected) for daytime periods (12:00–14:00 PM LT) is given in filled symbols (respectively open symbols). Simulations using both “forecast” (circles) and “climate” (squares) versions of REMO are presented.

Flask samples both at ground stations and at aircraft sites are collected preferentially during the day, which implies that over continents we must accordingly select the output of models. Aircraft sampling is additionally biased towards fair weather conditions. On the other hand, continuous stations record atmospheric CO₂ mixing ratio all day round, and thus are sensitive to night-time accumulation effects over continents. This is illustrated in Fig. 12 at the tall tower HUN by the observed difference of 7.2 ppmv at 115 m aboveground between the monthly averaged continuous record and the monthly average determined from daytime flask samples. We calculated monthly averaged CO₂ mixing ratios from “selected” daytime REMO output (12:00–14:00 LT) as well as from “unselected” output using all time steps.

Figure 12 compares the REMO results with observations. All data and models are arbitrarily referenced against the monthly value of the MHD station, because only CO₂ gradients among sites can be predicted by a model. For increasing latitudes over the North Atlantic (Fig. 2), a slight increase in CO₂ of 0.87 ppmv is observed between MHD (53°N) and ZEP (78°N), which is well captured in all the versions of REMO. Both REMO climate and forecast versions differ from the data by less than 0.5 ppmv in the way they predict the CO₂ latitudinal distribution over the ocean. We note also that the selected and unselected REMO output are close to each other over the ocean (<0.1 ppmv) because neither the air–sea fluxes nor the marine boundary layer height have a diurnal variation. Over Western Europe (ORL, SCH) REMO matches the observations within 1 ppmv (ORL, SCH). On the other hand, the composite set of ground stations and aircraft sites shows that there is a large CO₂ drop of 6 ppmv between Western Europe and Western Siberia. East of 30°E, however, all the data come from aircraft sites or mountain stations, with the exception of KZD, so that their CO₂ values reflect the attenuation of the summer sink signal with height over Eurasia (e.g. Nakazawa et al., 1997). If we had representative CO₂ measurements closer to the ground, their daytime CO₂ average value would be even more depleted as compared to ocean stations (Fig. 5). Indeed, the tall tower HUN record shows daytime CO₂ values that are 8 ppmv lower than the ocean baseline. REMO does not capture the West to East CO₂ drop in the lower troposphere. Since lower troposphere gradients necessarily reflect a large-scale signal, we must search an explanation which involves either an underestimate of the July biospheric sink over Eurasia, or an underesti-

mate in the July Northern Hemisphere sink, which is advected into REMO via its boundary conditions provided by TM3. Preliminary simulations with REMO and TURC of a full seasonal cycle of CO₂ and fluxes (Chevallard, 2001) suggest that the seasonal phase of NEE in TURC is incorrect, and produces too early a drawdown in spring followed by too rapid a build up in July.

In Figure 12 we observe that the daytime selection of REMO output applied at aircraft sites has no effect, because the diurnal cycle of CO₂ becomes attenuated above the boundary layer (Lloyd et al., 2001; Ramonet et al., 2002). In contrast, the daytime selection procedure is critical when matching model calculations and observations near the ground. At HUN, REMO does not reproduce the mean CO₂ value, but the difference between unselected and selected model output of 6.5 ppmv is close to the observed one of 7.2 ppmv. A similar effect of model selection is simulated at the ground level flask station KZD. Finally, the differences between the two versions of REMO increase over the interior of the Eurasian continent (up to 2 ppmv), reflecting differences in meteorology (section 2), but they remain small as compared to the mismatch between model and observations, which we attribute to incorrect biospheric fluxes. As an order of magnitude, we calculate that in order to bring REMO in agreement with the observed drop in CO₂, assuming a mean residence time of air of 5 d within the domain, an extra sink of 0.8 GtC would be needed in July over European Russia and western Siberia. That number translates into a flux of 46 gC m⁻² per month, which is about 20% of the annual primary productivity of western Siberian forests (Schultze et al., 1999). Part of the “missing sink” in REMO comes from the fact that we assumed an annually balanced biospheric flux. By doing so, we ignore the well characterised existence of a terrestrial carbon sink of 0.6–2.3 GtC per year in the Northern Hemisphere (IPCC, 2001) to which uptake in Boreal Asia may contribute as much as 0.5 ± 0.5 GtC per year (Gurney et al., 2002).

6. Conclusions

We simulated the spatial and temporal variations of CO₂ over the Eastern part of the North Atlantic, Western Europe and Western Siberia in July 1998 using the regional atmospheric model REMO. The spatial resolution of REMO is at least four times higher than the one of global models commonly used to

transport CO₂, which is desirable to account for the complex geography, meteorology and patterns of carbon sources and sinks in Europe. The variations in CO₂ result from atmospheric transport acting on surface fluxes. In this study, high-resolution Net Ecosystem Exchange fluxes predicted by the TURC model using satellite NDVI observations were transported and driven by the simulated meteorology. The simulated hourly Net Ecosystem Exchange compares well with pointwise eddy covariance measurements along an east to west transect in Siberia, European Russia, and Hungary. In particular, the amplitude of the diurnal cycle is correctly reproduced. The simulated CO₂ field was compared with atmospheric observations. Firstly, we found that REMO was capable of realistically reproducing the diurnal variation of CO₂ near the ground, close to vegetation, which results from the diurnal cycle of NEE being modulated by the diurnal growth of the atmospheric boundary layer. Near industrial regions it was also observed that fossil emissions can contribute to the CO₂ diurnal cycle. Secondly, we found that REMO was capable of correctly simulating the diurnal variability of CO₂ vertical profiles between the ground and 3000 m, as compared with intensive aircraft campaigns in European Russia and Siberia. Thirdly, using two versions of REMO, we found that a more realistic simulated synoptic meteorology systematically improved the simulation of CO₂. In addition, the fine resolution model REMO better reproduced the observations than the coarse resolution model TM3. The above optimistic conclusions, should, however, be tempered by some shortcomings. The monthly CO₂ drop of 6 ppmv observed in July 1998 between the North Atlantic Ocean and Western Siberia was totally absent in REMO. This model failure has two origins. Firstly, the geographic and mean seasonal patterns of the biospheric fluxes in TURC are probably incorrect, with part of the disagreement being due to the assumption of annually balanced biospheric fluxes. By doing so, we do not account for the proven existence of a terrestrial carbon sink over northern hemisphere land masses, with at least a fraction of it being located in Boreal Asia. Secondly, above the boundary layer, we found that horizontal CO₂ gradients are essentially reflecting the transport of lateral boundary conditions prescribed from TM3. Thus REMO acts merely as an interpolator of TM3 to simulate the mean gradients of CO₂ in the troposphere over Eurasia. In the future, simulations of a full seasonal cycle will be performed and compared with flux and atmospheric measurements to evaluate further the

performances of our modelling system. This study is a first step towards an integrated model in which the atmospheric and biospheric processes will be directly coupled. This will allow us to account for feedbacks between carbon, water and energy fluxes and atmospheric transport over continental areas. Also, regional inversions of carbon sources and sinks are underway using the REMO model.

7. Acknowledgements

We thank all the participants of the EUROSI-BERIAN CARBONFLUX project who provided their measurements and valuable advice. Thanks are also due to Zoltan Barcza, Hungary, for providing the measurements of the Hegyhátsál station, and Ralf Podzun, MPI Hamburg, for his helpful technical support concerning the REMO model. The work was funded by the European Commission under contract no. ENV4-CT97-0491 (EUROSIBERIAN CARBONFLUX). We thank the ECMWF for providing surface and model level analysis data. We also acknowledge the support of C. Boone (IPSL's Pole données) for extracting the data.

Appendix: Dataset of atmospheric CO₂ measurements

In this section we compare REMO with observations during July 1998, summarised in Table 5.

A.1. Mace Head, western Ireland (MHD)

Mace Head is located 5 m above sea level. Atmospheric CO₂ has been continuously measured at Mace Head since June 1992 (Bousquet et al., 1996; Biraud et al., 2000). The meteorological situation is mainly influenced by the westerly passage of frontal systems originating from the North Atlantic Ocean, which determines the CO₂ "baseline". Synoptic variations in the origin of air masses, from the North Atlantic or from Europe, induce changes in the CO₂ concentration, with large positive and sometimes negative anomalies (Biraud et al., 2000).

A.2. Schauinsland, south Germany (SCH)

The station is located 10 km south of Freiburg in the Black Forest on a mountain ridge about 100 m above the Rhine Valley. It is operated by the German Environment Agency, Berlin, and is part of the Global Atmosphere Watch (GAW) program of the World

Table 5. Summary description of atmospheric stations used in this study (Appendix)

Station	Code	Location	Altitude (asl)	Sampling	Characteristics
Mace Head	MHD	53° N, 10° W	5 m	Continuous	Coastal station, Atlantic
Schauinsland	SCH	48° N, 8° E	1205 m	Continuous	Mountain station, western Europe
Hegyhátsál	HUN	46° N, 16° E	248 m	Continuous	Tall tower, western Europe
Fyodorovskoye	TVR	56° N, 33° E	265 m	Continuous,	Short tower,
			300–3000 m	Aircraft	European Russia
Zotino	ZOT	60° N, 90° E	100 m	Continuous,	Short tower, central
			100–3000 m	Aircraft	Siberia
Baltic sea	BAL	55° N, 17° E	7 m	Flask	
Orléans	ORL	48° N, 1° E	100–3000 m	Aircraft flask	
Iceland	ICE	63° N, 20° W	100 m	Flask	
Kazakstan	KZD	44° N, 78° E	412 m	Flask	
Kazakstan	KZM	43° N, 78° E	2519 m	Flask	
Station "M"	STM	66° N, 2° E	7 m	Flask	
Spitzbergen	ZEP	79° N, 12° E	474 m	Flask	

Meteorological Organisation. During moderate or strong winds this station is shown to be representative for mean atmospheric CO₂ conditions over Western Europe (Schmidt et al., 2001; Schmidt et al., 1996; Levin et al., 1995).

A.3. Fyodorovskoye, European Russia (TVR)

Fyodorovskoye is located in the Central Forest Reserve, southern taiga, about 300 km north-west of Moscow. At this station three kinds of CO₂ concentration measurements are performed within the EUROSIBERIAN CARBONFLUX project: (1) two short towers of continuous eddy covariance NEE and CO₂ above the canopy over a 150-yr-old spruce forest and over a bog, (2) regular biweekly flask measurements between 200 and 3000 m and (3) vertical profiles of CO₂ during intensive observation periods (Milyukova et al., 2002; Arneth et al., 2002; Ramonet et al., 2002).

A.4. Zotino, central Siberia (ZOT)

Zotino is located 600 km north of the city of Krasnoyarsk close to the small village of Zotino, located at the Jenisey river. The region belongs to the north Siberian

taiga. Two short towers measure eddy covariance NEE and CO₂ concentration above the canopy (Lloyd et al., 2002 and Arneth et al., 2002). Aircraft measurements of CO₂ vertical profiles were performed on a regular basis and during intensive observation periods (Lloyd et al., 2002 and Styles et al., 2002).

A.5. Hegyhátsál, western Hungary (HUN)

Hegyhátsál (Haszpra, 1999; Haszpra et al., 2001; Barcza, 2001) is a tall tower located in a rural site in western Hungary. CO₂ vertical profiles are measured along a television transmission tower at 10, 48, 82 and 115 m. NEE has been measured since 1997 by an eddy correlation system placed at 82 m. The surroundings of the tower are covered by different agricultural fields and forest patches.

A.6. Flask sampling sites (MHD, STM, ICE, KZD, KZM, BAL, ZEP)

The NOAA CMDL Carbon Cycle Greenhouse Gases group has operated the cooperative air sampling network (<http://www.cmdl.noaa.gov/ccgg/flask/index.html>) since 1992. The sites used in this study are given in Table 5.

REFERENCES

- Ahrens, B., Karstens, U., Rockel, B. and Stuhmann, R. 1998. On the validation of the atmospheric model REMO with ISCCP data and precipitation measurements using simple statistics. *Meteorol. Atmos. Phys.* **68**, 127–142.
- Arneth, A., Kurbatova, J., Kolle, O., Shibistova, O., Lloyd, J., Vygodskaya, N. N. and Schulze, E.-D. 2002. Comparative ecosystem – atmosphere exchange of energy and mass in a European and a central Siberian bog. II. Interseasonal

- and interannual variability of CO₂ fluxes. *Tellus* **54B** (this issue).
- Barcza, Z. 2001. Long term atmosphere/biosphere exchange of CO in Hungary. PhD Thesis, Budapest, <http://nimbus.elte.hu/~bzoli/thesis/>.
- Biraud, S., Ciais, P., Ramonet, M., Simmonds, P., Kazan, V., Monfray, P., O'Doherty, S., Spain, T. G. and Jennings, S. G. 2000. European greenhouse gas emissions estimated from continuous atmospheric measurements and radon-222 at Mace Head, Ireland. *J. Geophys. Res.* **105**, D1, 1351–1366.
- Biraud, S., Ciais, P., Ramonet, M., Simmonds, P., Kazan, V., Monfray, P., O'Doherty, S., Spain, T. G. and Jennings, S. G. 2002. Quantification of carbon dioxide, methane, nitrous oxide and chloroform emissions over Ireland from atmospheric observations at Mace Head. *Tellus* **54**, 41–60.
- Bousquet, P., Gaudry, A., Ciais, P., Kazan, V., Monfray, P., Simmonds, P. G., Jennings, S. G. and O'Connor, T. C. 1996. Atmospheric CO₂ concentration variations recorded at Mace Head, Ireland, from 1992 to 1994. *Phys. Chem. Earth* **21**, 477–481.
- Chevillard, A., Ciais, P., Karstens, U., Heimann, M., Schmidt, M., Levin, I., Jacob, D. and Podzun, R. 2002. Transport of ²²²Rn using the regional model REMO: A detailed comparison with measurements over Europe. *Tellus* **54B** (this issue).
- Chevillard, A. 2001. Etude à haute résolution du CO₂ atmosphérique en Europe et en Sibérie. Impact pour les bilans de carbone. PhD Thesis, Université Pierre et Marie Curie, Paris, France.
- Ciais, P., Tans, P. P., Denning, A. S., Francey, R. J., Trolier, M., Meijer, H. A. J., White, J. W. C., Berry, J. A., Randall, D. A., Collatz, G. J., Sellers, P. J., Monfray, P., and Heimann, M. 1997. A three-dimensional synthesis study of delta O-18 in atmospheric CO₂. 2. Simulations with the TM2 transport model. *J. Geophys. Res.* **102**, D5, 5873–5883.
- Conway, T. J., Tans, P. P., Waterman, L. S., Thoning, K., Kitzis, D. R., Masarie, K. A. and Zhang, N. 1994. Evidence for interannual variability of the carbon cycle from the NOAA/CMDL global air sampling network. *J. Geophys. Res.* **99**, D11, 22831–22855.
- Denning, A. S., Randall, D. A., Collatz, G. J. and Sellers, P. J. 1996. Simulations of terrestrial carbon metabolism and atmospheric CO₂ in a general circulation model. Part 2: Simulated CO₂ concentrations. *Tellus* **48B**, 543–567.
- Engardt, M. and Holmén, K. 1999. Model simulations of anthropogenic-CO₂ transport to an Arctic monitoring station during winter. *Tellus* **51B**, 194–209.
- Guernsey, K. R., Law, R. M., Denning, S. A., Rayner, P. J., Baker, D. *et al.* 2002. Towards robust regional estimates of CO₂ sources and sinks using atmospheric transport models. *Nature* **415**, 620–630.
- GLOBALVIEW-CO₂. 2001. Cooperative Atmospheric Data Integration Project – Carbon Dioxide. CD-ROM, NOAA CMDL, Boulder Colorado [also available on Internet via anonymous FTP to <ftp.cmdl.noaa.gov>, Path: [cgg/co2/GLOBALVIEW](ftp://co2/GLOBALVIEW)].
- Hamelbeck, F., Haimberger L. and Hantel, M. 2001. Convection in PIDCAP part I: Evaluating LAM convection. *Meteorol. Atmos. Phys.* **77**, 85–98.
- Haszpra, L. 1999. On the representativeness of carbon dioxide measurements. *J. Geophys. Res.* **104**, D21, 26953–26960.
- Haszpra, L., Barcza, Z., Bakwin, P. S., Berger, B. W., Davis, K. J. and Weidinger, T. 2001. Measuring system for the long-term monitoring of biosphere/atmosphere exchange of carbon dioxide. *J. Geophys. Res.* **106**, D3, 3057–3069.
- Heimann, M. 1995. *The global tracer model TM2*, Technical Report No.10, Deutsches Klima Rechenzentrum, Hamburg, 47 pp.
- Hollmann, R., Mueller, J. and Stuhlmann, R. 2000. A regional earth radiation budget derived with ScaRaB for validation purposes in BALTEX. *Phys. Chem. Earth B* **25**, 69–72.
- IPCC 2001.
- Jacob, D. and Podzun, R. 1997. Sensitivity studies with the regional climate model REMO. *Meteorol. Atmos. Phys.* **63**, 119–129.
- Jacob, D., Van den Hurk, B. J. J. M., Andrae, U., Elgered, G., Fortelius, C., Graham, L. P., Jackson, S. D., Karstens, U., Köpken, C., Lindau, R., Podzun, R., Rockel, B., Rubel, F., Sass, B. H., Smith, R. N. B., and Yang, X. 2001. A comprehensive model inter-comparison study investigating the water budget during the BALTEX-PIDCAP period. *Meteorol. Atmos. Phys.* **77**, 19–43.
- Jürrens, R. 1999. Validation of surface fluxes in climate simulations of the Arctic with the regional model REMO. *Tellus* **51A**, 698–709.
- Karstens, U., Nolte-Holube, R. and Rockel, B. 1996. Calculation of the Water Budget over the Baltic Sea Catchment Area using the Regional Forecast Model REMO for June 1993. *Tellus* **48A**, 684–692.
- Kjellström, E., Holmén, K., Eneroth, K. and Engardt, M. 2002. Summertime Siberian CO₂ simulations with the regional transport model MATCH: A feasibility study of carbon uptake calculations from EUROSIB data. *Tellus* **54B** (this issue).
- Lafont, S., Kergoat, L., Dedieu, G., Chevillard, A., Kjellström, E., Karstens, U. and Kolle, O. 2002. Spatial and temporal variability of land CO₂ fluxes estimated with remote sensing and analysis data over western Eurasia. *Tellus* **54B** (this issue).
- Langmann, B. 2000. Numerical modelling of regional scale transport and photochemistry directly together with meteorological processes. *Atmos. Environ.* **34**, 3585–3598.
- Langmann, B. and Bauer, S. 2002. On the importance of reliable background concentrations of ozone for regional scale photochemical modelling. *J. Atmos. Chem.*, in press.
- Levin, I., Graul, R. and Trivett, N. B. A. 1995. Long-term observations of atmospheric CO₂ and carbon isotopes at continental sites in Germany. *Tellus* **47B**, 23–34.
- Lindau, R. and Ruprecht, E. 2000. SSM/I-derived total water vapour content over the Baltic Sea compared to independent data. *Meteorol. Z.* **9**, 117–123.
- Lloyd, J., Langenfelds, R., Francey, R. J., Gloor, M., Zolothukine, D., Tchekakova, N. M., Shibistova, O.,

- Allison, C. A., Brand, W. A., Werner, R. and Schulze, E.-D. 2002. A trace gas climatology above Zotino, central Siberia. *Tellus* **54B** (this issue).
- Lloyd, J., Francey, R. J., Mollicone, D., Raupach, M. R., Sogachev, A., Arneth, A., Byers, J. N., Kelliher, F. M., Rebmann, C., Valentini, R., Wong, S.-C., Bauer, G. and Schulze, E.-D. 2001. Vertical profiles, boundary layer budgets and regional flux estimates for CO₂ and its ¹³C/¹²C ratio for water vapor above a forest/bog mosaic in central Siberia. *Global Biogeochem. Cycles* **15**, 267–284.
- Louis, J.-F. 1979. A parametric model of vertical eddy fluxes in the atmosphere. *Bound. Layer Meteorol.* **17**, 187–202.
- Majewski, D. 1991. The Europamodell of the Deutscher Wetterdienst., ECMWF course “Numerical methods in atmospheric models”, 2, 147–191.
- Marland, G., Boden, T. A. and Andres, R. J. 2000. Global, Regional, and National CO₂ Emissions. In: *Trends: a compendium of data on global change. Carbon Dioxide Information Analysis Center, Oak Ridge National Laboratory* U.S. Department of Energy, Oak Ridge, Tenn., USA.
- Mellor, B. and Yamada, T. 1974. A hierarchy of turbulence closure models for planetary boundary layers. *J. Atmos. Sci.* **31**, 1791–1806.
- Milyukova, I., Kolle, O., Varlagin, A., Vygodskaya, N. N., Schulze, E.-D. and Lloyd, J. 2002. Carbon balance of a southern taiga spruce stand in European Russia. *Tellus* **54B** (this issue).
- Nakazawa, T., Sugawara, S., Inoue, G., Machida, T., Makshyutov, and Mukai, H. 1997. Aircraft measurements of the concentrations of CO₂, CH₄, N₂O and CO and the carbon and oxygen isotopic ratios of CO₂ in the troposphere over Russia. *J. Geophys. Res.* **102**, (D3), 3843–3859.
- Olivier, J. G. J., Bouwman, A. F., Van der Maas, C. W. M., Berdowski, J. J. M., Veldt, C., Bloos, J. P. J., Visschedijk, A. J. H., Zandyelt, P. Y. J. and Haverlag, J. L. 1996. Description of EDGAR Version 2.0. A set of global emission inventories of greenhouse gases and ozone-depleting substances for all anthropogenic and most natural sources on a per country basis and on 1 × 1 grid. RIVM/TNO report, December 1996. RIVM, Bilthoven, RIVM report nr. 771060 002. [TNO MEP report nr. R96/119].
- Ramonet, M., Ciais, P., Nepomniachii, I., Sidorov, K., Neubert, R. E. M., Picard, D., Kazan, V., Biraud, S., Gusti, M., Kolle, O., Schulze, E.-D. and Lloyd, J. 2002. Three years of aircraft based trace gas measurements over the Fyodoroskoye southern taiga forest, 300 km North-West of Moscow. *Tellus* **54B** (this issue).
- Rockel, B. and Karstens, U. 2001. Development of the water budget for three extra-tropical cyclones with intense rainfall over Europe. *Meteorol. Atmos. Phys.* **77**, 75–83.
- Roeckner, E., Arpe, K., Bengtsson, L., Christoph, M., Claussen, M., Duemenil, L., Esch, M., Giorgetta, M., Schlese, U. and Schulzweida, U. 1996. *The atmospheric general circulation model ECHAM-4: Model description and simulation of present-day climate*. MPI, Hamburg, Germany.
- Ruimy, A., Dedieu, G. and Saugier, B. 1996. TURC: a diagnostic model of continental gross primary productivity as net primary productivity, *Global Biogeochem. Cycles* **10**, 269–285.
- Schmidt, M., Graul, R., Sartorius, H. and Levin, I. 1996. Carbon dioxide and methane in continental Europe: A climatology, and ²²²Rn-based emission estimates. *Tellus* **48B**, 457–473.
- Schmidt, M., Glatzel-Mattheier, H., Sartorius, H., Worthy, D. E. and Levin, I. 2001. Western European N₂O emissions: A top-down approach based on atmospheric observations. *J. Geophys. Res.* **106**, D6, 5507–5516.
- Schrodin, R. 1993 (ed.): *Quarterly report of the Operational NWP-Models of the Deutscher Wetterdienst*. Available from the Deutscher Wetterdienst, Offenbach, Germany.
- Schultze, E.-D., Lloyd, J., Kelliher, F. M., Wirth, C., Rebmann, C., Lühker, B., Mund, M., Knohl, A., Milyukova, I., Schulze, W., Ziegler, W., Varlagin, A., Valentini, R., Sogachov, A., Valentini, R., Dore, S., Grigoriev, S., Kolle, O., Tchebakova, N., Vgodskaya, N. N. 1999. Productivity of forests in the Euro Siberian boreal region and their potential to act as a carbon sink – A synthesis. *Global Change Biology* **5**, 703–722.
- Smolarkiewicz, P. K. 1983. A simple positive definite advection scheme with small implicit diffusion. *Mon. Wea. Rev.* **111**, 479–486.
- Styles, J. M., Lloyd, J., Zolothukine, D., Lawton, K. A., Tchebakova, N., Francey, R. J., Arneth, A., Salamakho, D., Kolle, O. and Schulze, E.-D. 2002. Estimates of regional surface CO₂ exchange and carbon and oxygen isotope discrimination during photosynthesis from concentration profiles in the atmospheric boundary layer. *Tellus*, **54B** (this issue).
- Stull, R. B. 1988. *An introduction to boundary layer meteorology*. Kluwer Academic Publishers, Dordrecht, The Netherlands.
- Takahashi, T., Sutherland, S. C., Sweeney, C., Poisson, A., Metzler, N., Tilbrook, B., Bates, N., Wanninkhof, R., Feely, R. A., Sabine, C., Olafsson, J. and Nojiri, Y. 2002. Global sea–air CO₂ flux based on climatological surface ocean pCO₂, and seasonal biological and temperature effects. *Deep-sea Res.* **1008** (in press).
- Tiedtke, M. 1989. A comprehensive mass flux scheme for cumulus parameterization in large scale models. *Mon. Wea. Rev.* **117**, 1779–1800.
- van Meijgaard, E., Andrae, U. and Rockel, B. 2001. Comparison of model predicted cloud parameters and surface radiative fluxes with observations on the 100 km scale. *Meteorol. Atmos. Phys.* **77**, 109–130.
- Wanninkhof, R. 1992. Relationship between wind speed and gas exchange. *J. Geophys. Res.* **97**, 7373–7382.
- Zhang, Y., Rockel, B., Stuhlmann, R., Hollmann, R. and Karstens, U. 2001. REMO cloud modeling: Improvements and validation with ISCCP DX data. *J. Appl. Meteorol.* **40**, 389–408.